Quenching Mo optical losses in CIGS solar cells by a point contacted dual-layer dielectric spacer
A 3-D optical study

Rezaei, Nasim; Isabella, Olindo; Vroon, Zeger; Zeman, Miro

Important note
To cite this publication, please use the final published version (if applicable).
Please check the document version above.

Quenching Mo optical losses in CIGS solar cells by a point contacted dual-layer dielectric spacer: a 3-D optical study

Nasim Rezaei,[1,*] Olindo Isabella,[1] Zeger Vroon,[2] and Miro Zeman[1]

[1]*Delft University of Technology, Photovoltaic Materials and Devices, Mekelweg 4, 2628CD Delft, the Netherlands*
[2]*TNO-Brightlands Materials Center, Urmondsebaan 22, 6167 RD Geleen, PO BOX 18, 6160 MD Geleen, the Netherlands*
*n.rezaei@tudelft.nl

Abstract: A 3-D optical modelling was calibrated to calculate the light absorption and the total reflection of fabricated CIGS solar cells. Absorption losses at molybdenum (Mo) / CIGS interface were explained in terms of plasmonic waves. To quench these losses, we assumed the insertion of a lossless dielectric spacer between Mo and CIGS, whose optical properties were varied. We show that such a spacer with low refractive index and proper thickness can significantly reduce absorption in Mo in the long wavelength regime and improve the device's rear reflectance, thus leading to enhanced light absorption in the CIGS layer. Therefore, we optimized a realistic two-layer MgF_2 / Al_2O_3 dielectric spacer to exploit (i) the passivation properties of ultra-thin Al_2O_3 on the CIGS side for potential high open-circuit voltage and (ii) the low refractive index of MgF_2 on the Mo side to reduce its optical losses. Combining our realistic spacer with optically-optimized point contacts increases the implied photocurrent density of a 750 nm-thick CIGS layer by 10% for the wavelengths between 700 and 1150 nm with respect to the reference cell. The elimination of plasmonic resonances in the new structure leads to a higher electric field magnitude at the bottom of CIGS layer and justifies the improved optical performance.

References and links

1. D. Herrmann, P. Kratzert, S. Weeke, M. Zimmer, J. Djordjevic-Reiss, R. Hunger, P. Lindberg, E. Wallin, O. Lundberg, and L. Stolt, "CIGS module manufacturing with high deposition rates and efficiencies," in *2014 IEEE 40th Photovoltaic Specialist Conference* (PVSC) (IEEE, 2014), pp. 2775–2777.
2. H. Sugimoto, "High efficiency and large volume production of CIS-based modules," in *2014 IEEE 40th Photovoltaic Specialist Conference (PVSC)* (IEEE, 2014), pp. 2767–2770.
3. P. Jackson, R. Wuerz, D. Hariskos, E. Lotter, W. Witte, and M. Powalla, "Effects of heavy alkali elements in Cu(In,Ga)Se2 solar cells with efficiencies up to 22.6%," Phys. status solidi (RRL)-Rapid Res. Lett. **10**(8), 583–586 (2016).
4. M. A. Green, K. Emery, Y. Hishikawa, W. Warta, E. D. Dunlop, D. H. Levi, and A. W. Y. Ho-Baillie, "Solar cell efficiency tables (version 49)," Prog. Photovolt. Res. Appl. **25**(1), 3–13 (2017).
5. C. Onwudinanti, R. Vismara, O. Isabella, L. Grenet, F. Emieux, and M. Zeman, "Advanced light management based on periodic textures for Cu(In,Ga)Se$_2$ thin-film solar cells," Opt. Express **24**(6), A693–A707 (2016).
6. C. van Lare, G. Yin, A. Polman, and M. Schmid, "Light coupling and trapping in ultrathin Cu(In,Ga)Se$_2$ solar cells using dielectric scattering patterns," ACS Nano **9**(10), 9603–9613 (2015).
7. J. Krc, M. Sever, A. Campa, Z. Lokar, B. Lipovsek, and M. Topic, "Optical confinement in chalcopyrite based solar cells," Thin Solid Films, in press (2016).
8. J. Pettersson, T. Törndahl, C. Platzer-Björkman, A. Hultqvist, and M. Edoff, "The Influence of Absorber Thickness on Cu(In,Ga)Se Solar Cells With Different Buffer Layers," IEEE J. Photovoltaics **3**(4), 1376–1382 (2013).
9. Z. Jehl, F. Erfurth, N. Naghavi, L. Lombez, I. Gerard, M. Bouttemy, P. Tran-Van, A. Etcheberry, G. Voorwinden, and B. Dimmler, "Thinning of CIGS solar cells: Part II: Cell characterizations," Thin Solid Films **519**(21), 7212–7215 (2011).
10. E. Jarzembowski, M. Maiberg, F. Obereigner, K. Kaufmann, S. Krause, and R. Scheer, "Optical and electrical characterization of Cu(In,Ga)Se$_2$ thin film solar cells with varied absorber layer thickness," Thin Solid Films

576, 75–80 (2015).

11. K. Orgassa, H. W. Schock, and J. H. Werner, "Alternative back contact materials for thin film Cu(In,Ga)Se$_2$ solar cells," Thin Solid Films **431**, 387–391 (2003).

12. T. Hara, T. Maekawa, S. Minoura, Y. Sago, S. Niki, and H. Fujiwara, "Quantitative Assessment of Optical Gain and Loss in Submicron-Textured CuIn$_{1-x}$Ga$_x$Se$_2$ Solar Cells Fabricated by Three-Stage Coevaporation," Phys. Rev. Appl. **2**(3), 34012 (2014).

13. B. Vermang, J. T. Wätjen, V. Fjällström, F. Rostvall, M. Edoff, R. Gunnarsson, I. Pilch, U. Helmersson, R. Kotipalli, and F. Henry, "Highly reflective rear surface passivation design for ultra-thin Cu(In,Ga)Se$_2$ solar cells," Thin Solid Films **582**, 300–303 (2015).

14. B. Vermang, V. Fjällström, J. Pettersson, P. Salomé, and M. Edoff, "Development of rear surface passivated Cu(In,Ga)Se$_2$ thin film solar cells with nano-sized local rear point contacts," Sol. Energy Mater. Sol. Cells **117**, 505–511 (2013).

15. P. Casper, R. Hünig, G. Gomard, O. Kiowski, C. Reitz, U. Lemmer, M. Powalla, and M. Hetterich, "Optoelectrical improvement of ultra-thin Cu(In,Ga)Se$_2$ solar cells through microstructured MgF$_2$ and Al$_2$O$_3$ back contact passivation layer," Phys. status solidi (RRL)-Rapid Res. Lett. **10**(5), 376–380 (2016).

16. Z. C. Holman, A. Descoeudres, S. De Wolf, and C. Ballif, "Record infrared internal quantum efficiency in silicon heterojunction solar cells with dielectric/metal rear reflectors," IEEE J. Photovoltaics **3**(4), 1243–1249 (2013).

17. V. Demontis, C. Sanna, J. Melskens, R. Santbergen, A. H. M. Smets, A. Damiano, and M. Zeman, "The role of oxide interlayers in back reflector configurations for amorphous silicon solar cells," J. Appl. Phys. **113**(6), 64508 (2013).

18. Z. C. Holman, S. De Wolf, and C. Ballif, "Improving metal reflectors by suppressing surface plasmon polaritons: a priori calculation of the internal reflectance of a solar cell," Light Sci. Appl. **2**(10), e106 (2013).

19. B. Vermang, J. T. Wätjen, V. Fjällström, F. Rostvall, M. Edoff, R. Kotipalli, F. Henry, and D. Flandre, "Employing Si solar cell technology to increase efficiency of ultra-thin Cu(In,Ga)Se$_2$ solar cells," Prog. Photovolt. Res. Appl. **22**(10), 1023–1029 (2014).

20. B. Vermang, J. T. Wätjen, C. Frisk, V. Fjällström, F. Rostvall, M. Edoff, P. Salomé, J. Borme, N. Nicoara, and S. Sadewasser, "Introduction of Si PERC Rear Contacting Design to Boost Efficiency of Cu(In,Ga)Se Solar Cells," IEEE J. Photovoltaics **4**(6), 1644–1649 (2014).

21. O. Lundberg, M. Bodegård, J. Malmström, and L. Stolt, "Influence of the Cu(In,Ga)Se$_2$ thickness and Ga grading on solar cell performance," Prog. Photovolt. Res. Appl. **11**(2), 77–88 (2003).

22. M. Burghoorn, B. Kniknie, J. van Deelen, M. Xu, Z. Vroon, R. van Ee, R. van de Belt, and P. Buskens, "Improving the efficiency of copper indium gallium (Di-) selenide (CIGS) solar cells through integration of a moth-eye textured resist with a refractive index similar to aluminum doped zinc oxide," AIP Adv. **4**(12), 127154 (2014).

23. H. Raether, *Surface Plasmons on Smooth Surfaces* (Springer, 1988).

24. S. A. Maier, *Plasmonics: Fundamentals and Applications* (Springer Science & Business Media, 2007).

25. L. Novotny and B. Hecht, *Principles of Nano-Optics* (Cambridge University Press, 2012).

26. F.-J. Haug, T. Söderström, O. Cubero, V. Terrazzoni-Daudrix, and C. Ballif, "Influence of the ZnO buffer on the guided mode structure in Si/ZnO/Ag multilayers," J. Appl. Phys. **106**(4), 44502 (2009).

27. J.-H. Yoon, S. Cho, W. M. Kim, J.-K. Park, Y.-J. Baik, T. S. Lee, T.-Y. Seong, and J. Jeong, "Optical analysis of the microstructure of a Mo back contact for Cu(In,Ga)Se$_2$ solar cells and its effects on Mo film properties and Na diffusivity," Sol. Energy Mater. Sol. Cells **95**(11), 2959–2964 (2011).

28. O. Isabella, S. Solntsev, D. Caratelli, and M. Zeman, "3-D optical modeling of thin-film silicon solar cells on diffraction gratings," Prog. Photovolt. Res. Appl. **21**(1), 94–108 (2013).

29. A. Smets, K. Jäger, O. Isabella, R. van Swaaij, and M. Zeman, *Solar Energy: The Physics and Engineering of Photovoltaic Conversion, Technologies and Systems* (UIT Cambridge Limited, 2016).

30. R. Santbergen, H. Tan, M. Zeman, and A. H. M. Smets, "Enhancing the driving field for plasmonic nanoparticles in thin-film solar cells," Opt. Express **22**(104 Suppl 4), A1023–A1028 (2014).

31. F. Mollica, J. Goffard, M. Jubault, F. Donsanti, S. Collin, A. Cattoni, L. Lombez, N. Naghavi, R. Edf, I. Umr, and D. Renaissance, "Comparative study of patterned TiO$_2$ and Al$_2$O$_3$ layers as passivated back-contact for ultra-thin Cu(In,Ga)Se$_2$ solar cells," in *Photovoltaic Specialists Conference* (PVSC) (IEEE, 2016), pp. 6–10.

32. G. Dingemans and W. M. M. Kessels, "Status and prospects of Al$_2$O$_3$-based surface passivation schemes for silicon solar cells," J. Vac. Sci. Technol. A Vacuum, Surfaces, Film **30**(4), 40802 (2012).

33. M. J. Dodge, "Refractive properties of magnesium fluoride," Appl. Opt. **23**(12), 1980–1985 (1984).

34. O. Poncelet, R. Kotipalli, B. Vermang, A. Macleod, L. A. Francis, and D. Flandre, "Optimisation of rear reflectance in ultra-thin CIGS solar cells towards> 20% efficiency," Sol. Energy **146**, 443–452 (2017).

35. Z. C. Holman, M. Filipič, A. Descoeudres, S. De Wolf, F. Smole, M. Topič, and C. Ballif, "Infrared light management in high-efficiency silicon heterojunction and rear-passivated solar cells," J. Appl. Phys. **113**(1), 13107 (2013).

36. F.-J. Haug, T. Söderström, O. Cubero, V. Terrazzoni-Daudrix, and C. Ballif, "Plasmonic absorption in textured silver back reflectors of thin film solar cells," J. Appl. Phys. **104**(6), 64509 (2008).

37. B. Vermang, V. Fjällström, X. Gao, and M. Edoff, "Improved Rear Surface Passivation of Cu(In,Ga)Se$_2$ Solar Cells: A Combination of an Al$_2$O$_3$ Rear Surface Passivation Layer and Nanosized Local Rear Point Contacts," IEEE J. Photovoltaics **4**(1), 486–492 (2014).

38. G. Brown, V. Faifer, A. Pudov, S. Anikeev, E. Bykov, M. Contreras, and J. Wu, "Determination of the minority carrier diffusion length in compositionally graded Cu(In,Ga)Se$_2$ solar cells using electron beam induced current," Appl. Phys. Lett. **96**(2), 22104 (2010).
39. O. Isabella, *Light Management in Thin-Film Silicon Solar Cells* (TU Delft, Delft University of Technology 2013).

1. Introduction

Copper Indium Gallium (di)Selenide (CIGS) photovoltaic (PV) technology enables high performance thin-film solar cells [1–4], owing to its high absorption coefficient and gallium (Ga) content-based bandgap variation [5, 6]. To increase the PV market share of CIGS solar cells, larger and better industrial throughput is pursued by further improving the conversion efficiency and reducing cell-to-module losses. Also, for reducing material consumption (especially indium) and hence, achieving cheaper devices [7,8], the absorber thickness should be reduced from the standard 2-3 μm [3,5] to less than 1 μm.

However, reducing the absorber thickness results in less light absorption, more recombination at the back contact (as more charge carriers are created near the back contact) and shunting problems [6,8-10]. Furthermore, molybdenum (Mo) is a low-reflective metal [11,12] and Mo / CIGS interface is a highly recombinative interface [13]. While the surface recombination problem has been addressed by using a thin Al$_2$O$_3$ passivating film [14,15], the light management at such interface to compensate the current density loss in ultra-thin CIGS solar cells is still an issue, especially with industrially-compatible solutions in mind.

In both wafer-based and thin-film silicon (Si) technology, a low refractive index dielectric material (called *spacer layer*), placed between the metallic back reflector and the absorber, blue-shifts metal-related plasmonic resonances, increasing the short-circuit current density of the solar cell [16–18]. In this work, first, a physical explanation of the optical loss mechanism occurring at Mo / CIGS interface is provided. Then, borrowing the concept of dielectric spacer from Si PV technology, an intermediate dual-layer MgF$_2$ / Al$_2$O$_3$ stack [19] sandwiched between Mo back contact and CIGS layer is designed and optimized, using a three dimensional (3-D) optical modelling, based on the finite element method [5]. The insertion of such stack quenches the abovementioned optical losses, showing its effect in the improved implied photocurrent density (J_{ph}) in a solar cell with 1600 nm-thick CIGS layer. It is expected to boost also the open-circuit voltage (V_{OC}), owing to the rear passivation of CIGS layer operated by the Al$_2$O$_3$ thin film [19,20].

For carrier collection at the back contact, local point contacts are considered in an ultra-thin solar cell with a 750 nm-thick CIGS absorber. Both the dual-layer dielectric spacer and the geometry of the point contacts scheme are optimized, considering J_{ph} as the performance indicator.

2. Optical modelling

Ansoft® High Frequency Structure Simulator (HFSS), which is a 3-D Maxwell equation solver, was used for our optical studies. The optical constants of the materials composing different layers were imported into HFSS as inputs. The model was perpendicularly excited by means of plane waves through a Floquet port terminating a 300 nm-thick vacuum cushion above the top transparent conductive oxide (TCO). Master-slave boundary conditions were enforced on the sides of the unit cell, respectively aligned with xz- and yz- planes. S-parameters were used for the calculation of total reflectance ($R = |S_{11}|^2$). HFSS proprietary meshing algorithm was deployed, resulting in higher number of tetrahedra per unit volume in parts of the model with higher extinction coefficient and/or characterized by sudden change in real part of the refractive index (i.e. the more metallic and/or the thinner the layer is, the denser its mesh results). The absorption in each layer was calculated as [5]:

$$A_i(\lambda) = \frac{1}{2}\varepsilon_0 \, \mathrm{Im}\left(\varepsilon_i(\lambda)\right) \omega \int_{V_i} \left|\bar{E}(\lambda)\right|^2 dV \qquad (1)$$

where λ is the wavelength of light, ε_0 is the electric permittivity *in vacuo*, ω is the angular frequency, $\bar{E}$ is the electric field and ε_i and V_i are the relative electric permittivity and the volume of *i*-th layer, respectively. The real and imaginary parts of relative electric permittivity of the materials used in the model are plotted in Fig. 1.

For the simulated model to properly represent the fabricated solar cells, the simulation results should match the measured parameters with small deviation. In this respect, software calibration is an essential part of each simulation study. The thicknesses of the layers composing the simulated model were adjusted and the results (absorption and reflection spectra) were compared to the measured external quantum efficiency (EQE) and reflectance (*R*) of baseline cells fabricated at TNO [22]. The calibrated model is depicted in Fig. 2(a).

According to the method established in [5], periodic truncated pyramids were used to model the natural roughness of the CIGS layer, while also the conformal growth of top layers on CIGS was considered. The period of features modelling roughness of CIGS absorber is 330 nm, equal to the correlation length of a CIGS sample measured by atomic force microscopy. The presence of nanotextures on Mo surface is considered by implementing nano-sized features with bottom base area and height size of 30×30 nm^2 and 30 nm, respectively, and top base area of 20×20 nm^2 at Mo / CIGS interface, as shown in Fig. 2(a). It should be noted that no antireflective coating has been used in either the measured or the simulated devices.

In Fig. 2(b), experimental 1-*R* and EQE spectra are overlaid on the simulated reflectance and absorption spectra of the corresponding layers shown in Fig. 2(a). In the wavelength range between 450 and 950 nm, the light absorption in the simulated CIGS layer is more than the measured EQE, which can be due to carrier collection issues in the real device, resulting in recombination of electrons and holes before being collected at the terminals. The average difference between the simulated CIGS absorption and measured EQE was 0.056, while this average difference in *R* was 0.03. These results are in line with previously published modelling works [5]. In this study, we worked on improving the optical properties of the Mo / CIGS interface, that is reached only by low energy photons. For this reason, our priority was to achieve a reasonable spectral matching between measured and simulated spectra in the long wavelength range. As Fig. 2(b) shows, in the wavelength range between 900 and 1200 nm, the simulated 1-*R* and EQE spectra follow the same trend as their measured counterparts.

The presence of optical losses due to high absorption in Mo layer in the long wavelength range is well pronounced in Fig. 2(b). These optical losses near the bandgap of CIGS deteriorate the current generation of the solar cell and need to be quenched.
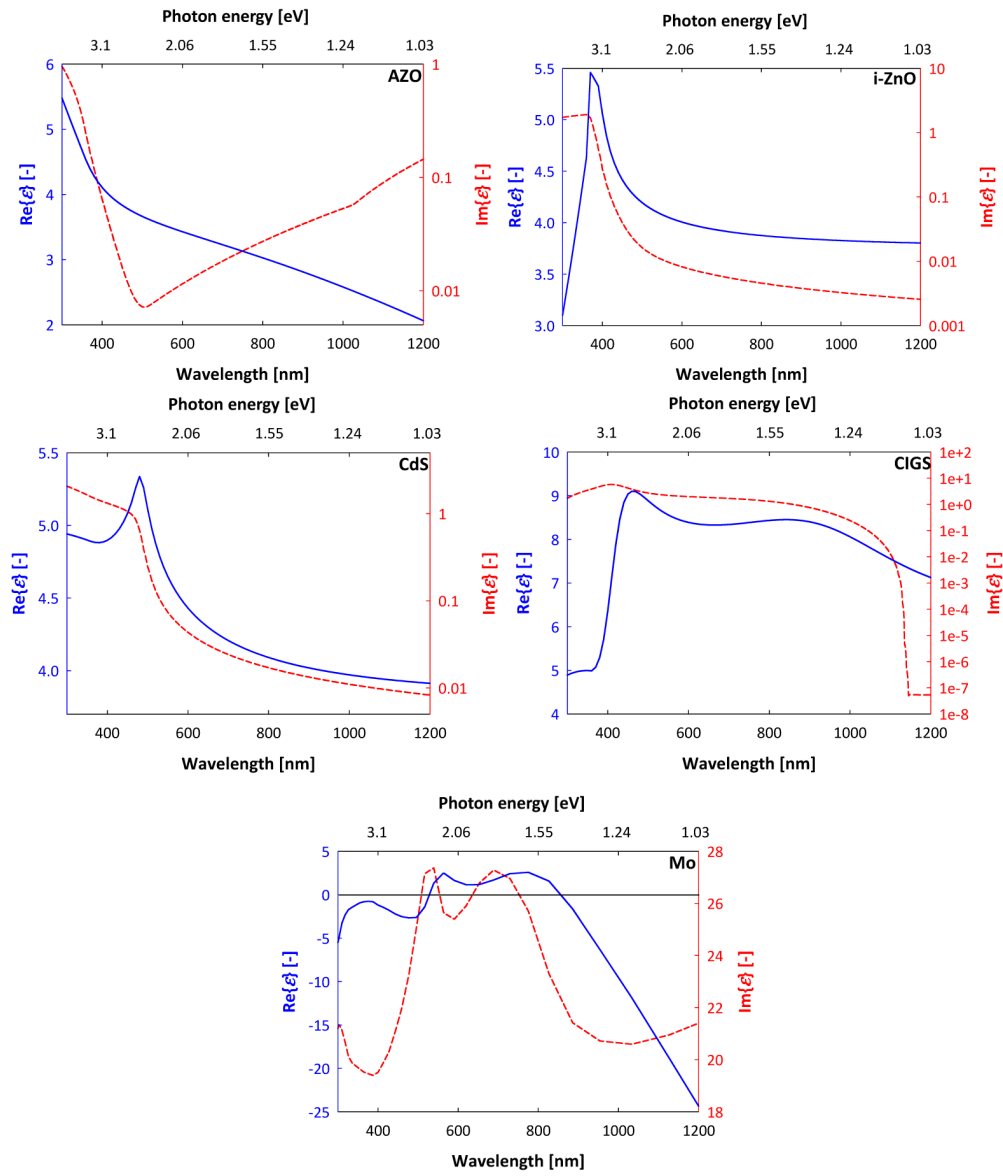
Fig. 1. Real (solid) and imaginary (dashed) parts of relative electric permittivity of materials used for the calibrated model as a function of wavelength (the first four optical properties are obtained from [21] and Mo from [5]).
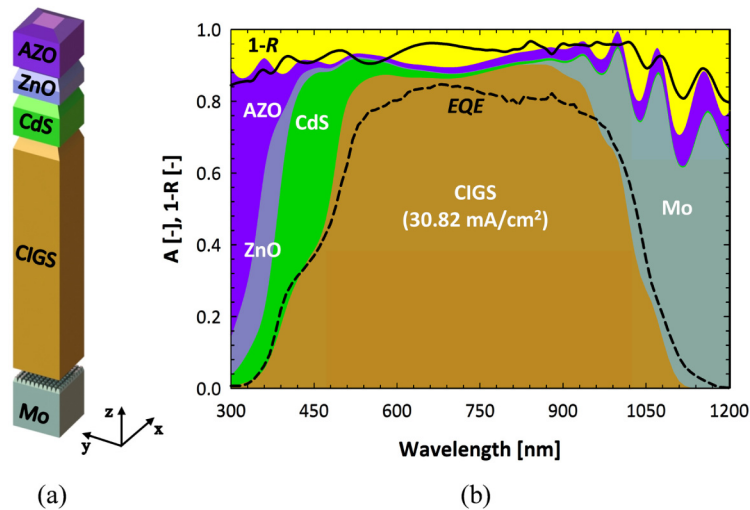
Fig. 2. a) Software model. Thicknesses of layers from top to bottom are (in nm): 250, 60, 70, 1600 and 320. b) Simulation results are compared to the measured EQE and 1-*R* (dashed and solid black curves, respectively). Colored areas indicate absorption in different layers of the structure.

3. Results and discussion

3.1 Nature of optical losses at the back contact

The nature of optical losses at the interface between Mo and CIGS is addressed here. Depending on the polarization of light impinging on a metal / dielectric interface, the interaction with metal's electron plasma leads to the excitation of surface plasmons (SPs) [23–25]. SPs can either be *surface-bound* or *leaky*. Surface-bound SPs (also known as surface plasmon polaritons, SPPs) propagate along the interface with maximum amplitude at the surface and exponential decay in the direction normal to the interface. Necessary conditions for exciting SPPs are (i) transverse magnetic polarized illumination light, (ii) real parts of electric permittivity of the two media having opposite signs and (iii) $|\text{Re}\{\varepsilon_m\}| > \text{Re}\{\varepsilon_d\}$, where ε_m and ε_d are the relative electric permittivity of metal and dielectric, respectively [25,26]. In addition, since SPPs cannot be directly excited by light incident on a flat interface through the dielectric medium, certain phase-matching conditions must occur, such as having a textured interface between metal and dielectric [23,24,26]. In case of Mo / CIGS interface, considering the whole wavelength range from 300 nm to 1200 nm, the necessary conditions for the excitation of SPPs are met between 980 nm and 1200 nm (Fig. 3(a)). On the other hand, if $|\text{Re}\{\varepsilon_m\}| < \text{Re}\{\varepsilon_d\}$, leaky SPs will be excited. In other words, when the $|\text{Re}\{\varepsilon_m\}|$ is smaller than the $\text{Re}\{\varepsilon_d\}$, the conditions for the excitation of a propagating wave component in the direction normal to the interface are met. It means that the wave propagates not only along but also normal to the interface and effectively, the SPs are not *confined* to the interface. To distinguish between the wavelength regions of bound and leaky surface waves, the *dispersion relation*, which describes the wave vector component parallel to the interface, is compared to the light line in the dielectric.

In a Cartesian coordinate system, we assume two half spaces, one metallic and one dielectric, where the plane $z = 0$ coincides with the interface between the two media. The dispersion relation is function of material properties and wavelength and can be derived as [23,24]:

$$\beta(\lambda) = k_0 \sqrt{\frac{\varepsilon_d \varepsilon_m}{\varepsilon_d + \varepsilon_m}} \qquad (2)$$

where β is the wave vector component parallel to the interface and $k_0 = 2\pi/\lambda$ is the wave vector of a photon *in vacuo*. In this relation, material properties such as damping and frequency dependency are considered. The light line in the dielectric represents instead the transverse component of the wave vector within a dielectric medium and is defined as $k_d = \mathrm{Re}\left\{ (2\pi/\lambda)\sqrt{\varepsilon_d} \right\}$. In Fig. 3(b), the real part of β at a Mo / CIGS interface is compared to the light line of CIGS in the wavelength range $300 < \lambda < 1200$ nm. Due to the wavelength dependency of $\varepsilon_{\mathrm{CIGS}}$, the light line of CIGS is not linear. The imaginary part of β, which is a measure of attenuation along the interface, is not shown here.
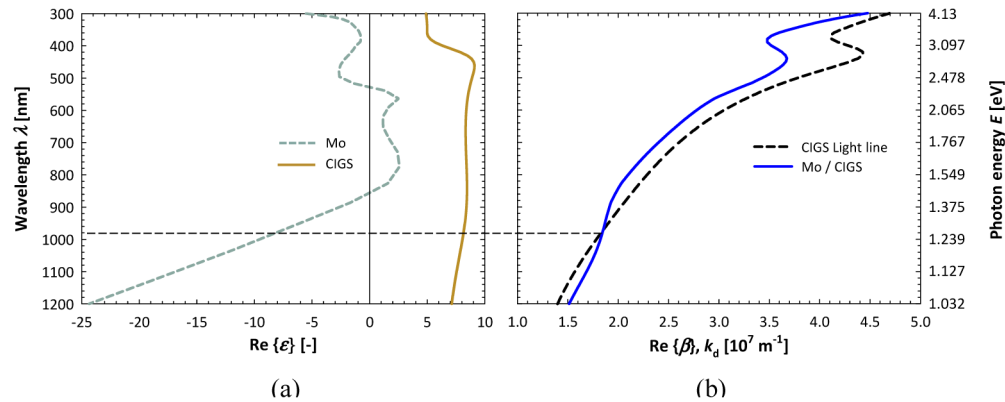

Fig. 3. a) Real part of relative electric permittivity of Mo (dashed) and CIGS (solid), and b) SPP dispersion curve at the interface between Mo and CIGS (blue) half spaces compared to CIGS light line (dashed black) as a function of wavelength (i.e. photon energy).

In Fig. 3(b), two wavelength ranges can be individuated. In the first one, where only SPPs may exist between Mo and CIGS ($980 < \lambda < 1200$ nm), the dispersion curve lies on the right-hand side of light line. For a perfectly flat interface, as the wave vector of SPPs is larger than the wave vector of the light of the same energy propagating along the interface [23], no SPP is allowed. However, the presence of self-grown nano-roughness on Mo surface [27] fulfills the conservation of momentum and energy [26], making the excitation of SPPs in a real CIGS solar cell possible in this wavelength range. This phenomenon will be investigated further for one example wavelength in section 3.4. The coupling of light into SPPs at the back contact surface is a source of optical loss, since these type of surface waves are strongly confined to the interface and will not lead to charge carrier generation in the absorber layer. In the second wavelength range (300 nm $< \lambda < 980$ nm), where only leaky surface waves can exist at Mo / CIGS interface, the wave vector of leaky SPs is smaller than the wave vector of light of the same energy propagating in CIGS. This means that even at a flat interface, these waves can be excited. Consequently, a large part of the light impinging on Mo surface, depending on the thickness of CIGS layer, will be absorbed in the Mo layer. Such optical loss is made even more serious, due to relatively higher real part of refractive index of Mo compared to more reflective metals such as silver, thus developing low reflectivity at the interface between Mo and CIGS.

3.2 Synthetic dielectric spacer

After having looked at the nature of optical losses at the back contact, an ideal lossless (i.e. *synthetic*) dielectric spacer is studied here to tackle this problem and boost the photo-current density of the solar cell. The electric permittivity (ε) and the thickness (d) of a synthetic

material sandwiched between Mo and CIGS were therefore varied in the wavelength range between 900 and 1200 nm and their influence on the optical performance of the solar cell was investigated. The choice of this wavelength range is related to the absorption in Mo in a 1600 nm-thick CIGS solar cell, as shown in Fig. 2(b).

For the remainder of this paper, a *synthetic* material is an ideal material with the imaginary part of the electric permittivity forcibly set to zero at all wavelengths ($\mathrm{Im}\{\varepsilon\} = 0 \,\forall\lambda$), while a *real* material is an actual material, characterized by its own wavelength-dependent complex electric permittivity ε. With respect to the calibrated model, aside the insertion of the synthetic dielectric spacer, all other structural parameters were kept the same.

Fig. 4. Modified model with the synthetic dielectric spacer layer. Thicknesses of different layers (in nm) from top to bottom are as follows: 250, 60, 70, 1600, *d* and 320. The thickness *d* of the spacer layer was varied between 20 nm and 170 nm.

J was employed as performance indicator. This parameter is either the photocurrent density generated in the absorber layer or the absorption loss in each supporting layer, integrated as photocurrent density. J can be calculated as follows [28]:

$$J_i = -q \int A_i(\lambda)\Phi(\lambda)\,d\lambda \qquad (3)$$

where i is the i-th analyzed layer, q is the electric charge, $A_i(\lambda)$ and $\Phi(\lambda)$ are the wavelength-dependent absorptance and AM1.5 photon flux [29], respectively. In this regard, $J_{\mathrm{ph}} = J_{\mathrm{CIGS}}$. Likewise, the current loss due to the total reflection (J_R) is calculated by replacing $A_i(\lambda)$ with $R(\lambda)$ in Eq. (2). Figure 4 depicts a visual rendering of the modelled solar cell endowed with a dielectric spacer.

In Fig. 5, contour plots of the absorption (integrated as current density) in Mo and CIGS ($d_{\mathrm{CIGS}} = 1600$ nm) in the wavelength range between 900 nm and 1200 nm as a function of spacer thickness and electric permittivity are shown. It can be concluded that the lower the refractive index of the spacer layer ($n = \sqrt{\varepsilon}$) is, the higher the absorption is in the CIGS layer and vice versa in the Mo layer. *Real* low refractive index dielectric materials suitable as spacer are, for example, MgF_2, LiF, SiO_2, Al_2O_3 and TiO_2. Since the field reflected at the interface metal / dielectric spacer forms a standing wave [30], it is important to set the proper thickness of the spacer so that the intensity of the wave travelling back to the absorber is at maximum. As Fig. 5(b) shows, for each spacer material, there is an optimal thickness at which J_{ph} can be maximized. This is in agreement with the findings of Holman *et al.* about the effect of spacer thickness on the internal reflectance improvement of Si-based solar cells [18],

stating that beyond a certain spacer thickness, the internal reflection (and hence, the photon absorption in the absorber) does not improve anymore.
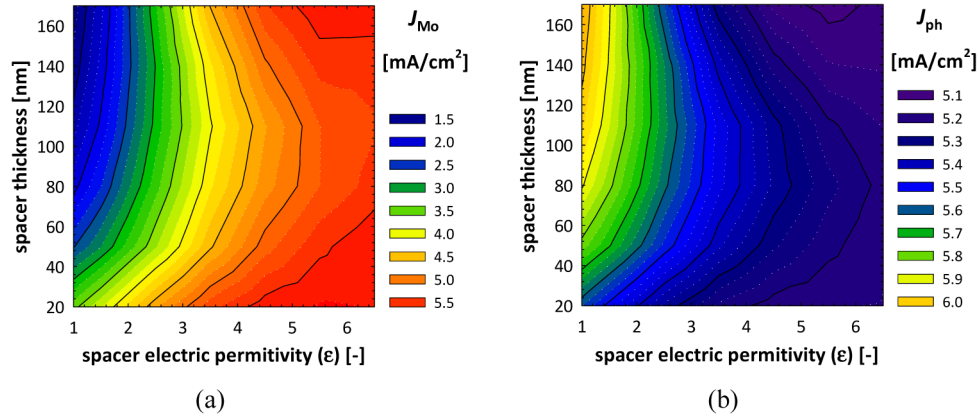

Fig. 5. Contour plots of the synthetic dielectric spacer optimization: a) integrated Mo absorption loss (J_{Mo}), and b) implied photo-current density in CIGS layer (J_{ph}) versus spacer thickness and electric permittivity for the wavelength range 900-1200 nm.

3.3 Al₂O₃ vs MgF₂

In CIGS solar cell architecture similar to a Si-based passivated emitter and rear cell (*PERC-like*) [20], a ~10-nm thick dielectric spacer is used to passivate the rear surface of CIGS, leading to an increase in V_{OC}. Al$_2$O$_3$ with an electric permittivity of 2.7 (or $n = \sqrt{\varepsilon} = 1.64$) at $\lambda = 1000$ nm is currently the state-of-the-art material from electrical point of view for rear surface passivation of CIGS solar cells [13, 31]. However, as it can be concluded from our theoretical optical study (Fig. 5(b)), a very thin layer of Al$_2$O$_3$ cannot perform well in increasing the short-circuit current density (J_{SC}) with respect to other materials with refractive indices less than that of Al$_2$O$_3$. MgF$_2$ with $\varepsilon = 1.87$ (or $n = \sqrt{\varepsilon} = 1.38$) at $\lambda = 1000$ nm is a good candidate for this purpose.

In Fig. 6, when Al$_2$O$_3$ with *real* material properties [32] is used as the spacer, the integrated absorption in the wavelength range between 900 and 1200 nm in different layers of CIGS solar cell as a function of d is shown. The first column indicates the simulation results of the reference cell in which no spacer is implemented. The results of Fig. 6 confirm that a thin layer of Al$_2$O$_3$ spacer (10 nm, for instance) does not lead to a significant increase in J_{ph}. Nevertheless, for the optimal thickness of 120 nm, an improvement of 0.42 mA/cm^2 in J_{ph} can be achieved. On the other hand, Fig. 7 shows that when MgF$_2$ [33] is used as the spacer material, at the optimal thickness of 140 nm, the enhancement of J_{ph} is 0.61 mA/cm^2 confirming the statement that a material with low refractive index and lower than that of Al$_2$O$_3$ is better for quenching Mo optical losses at the rear side of the solar cell [16]. These results are in good agreement with the findings of Poncelet *et al.* in [34], whereas a dielectric spacer is used to increase the rear reflectance of CIGS solar cells. However, we will show that when a different figure of merit than reflectance is used and for cells with thin CIGS layers, the optimized spacer thickness might be different.

A proper way of combining the advantages of Al$_2$O$_3$ and MgF$_2$ is to make a double-layer, in which an MgF$_2$ spacer layer with optimized thickness is covered by a thin Al$_2$O$_3$ layer (10 nm), potentially acting as a passivator to enhance V_{OC} (see Fig. 8). The feasibility of such a stack, in combination with local point contacts, has been shown in [19].
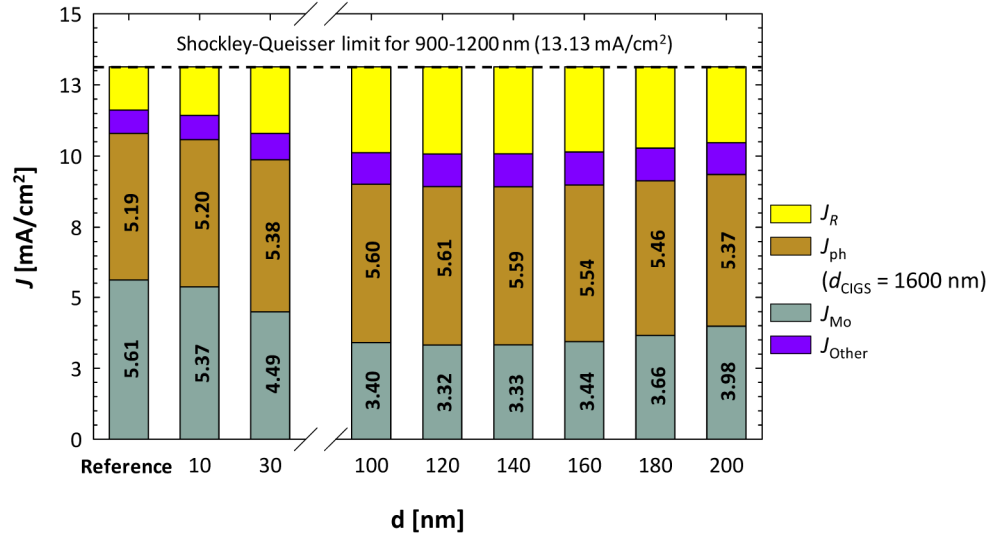
Fig. 6. Integrated absorption (or photocurrent density) in different layers of CIGS solar cell as a function of spacer thickness d in the wavelength range between 900 and 1200 nm when Al_2O_3 is used as the spacer.
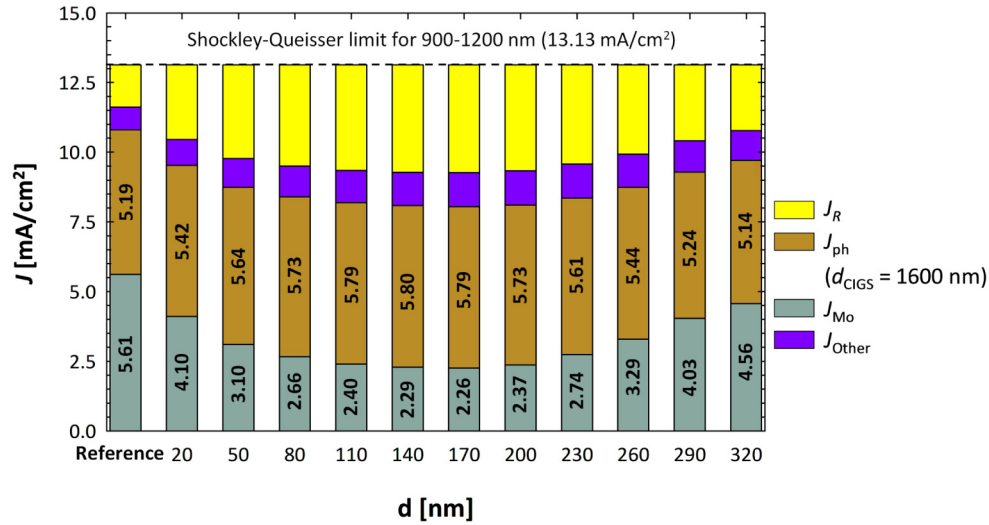

Fig. 7. Integrated absorption (or photocurrent density) in different layers of CIGS solar cell as a function of spacer thickness d in the wavelength range between 900 and 1200 nm when MgF_2 is used as the spacer.
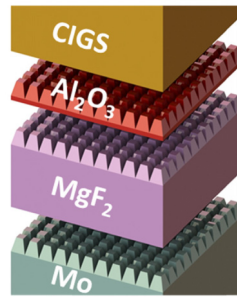
Fig. 8. The schematic of the two-layer dielectric spacer / passivating stack consisting of MgF$_2$ (140 nm) and Al$_2$O$_3$ (10 nm) placed between Mo back contact and CIGS absorber.

As mentioned before, the thickness optimization of the spacer is of great importance. Hence, the thickness of MgF$_2$ in the new stack was optimized to achieve the maximal J_{ph}. The results show that despite the presence of a 10 nm-thick Al$_2$O$_3$ layer on top of MgF$_2$, 140 nm is again the optimal thickness leading to the absorption spectrum shown in Fig. 9(a). In this figure, the increase (decrease) of absorption in CIGS (Mo) in the presence of the spacer can be clearly recognized. The absorption in the short wavelength range is not influenced by the presence of the spacer, since, for the absorber thickness of interest, the high-energy photons do not reach the back contact. A 0.63 mA/cm^2 improvement in J_{ph} for the whole visible spectrum can be obtained with this configuration (see Fig. 9b)). This is not a marginal improvement, given that it is achieved by simply depositing two layers on Mo and not by texturing the backside of the CIGS device, potentially leading to the growth of low quality CIGS and/or parasitic absorption.

It should be noted that in such structure, the total reflection will also increase, basically hindering the net effect of quenching Mo-related losses. This is the result of the increase in the secondary escape reflection [35] representing the photons that enter the cell, undergo one or more internal reflections and finally escape from the front side of the cell without being absorbed.

(a)   (b)
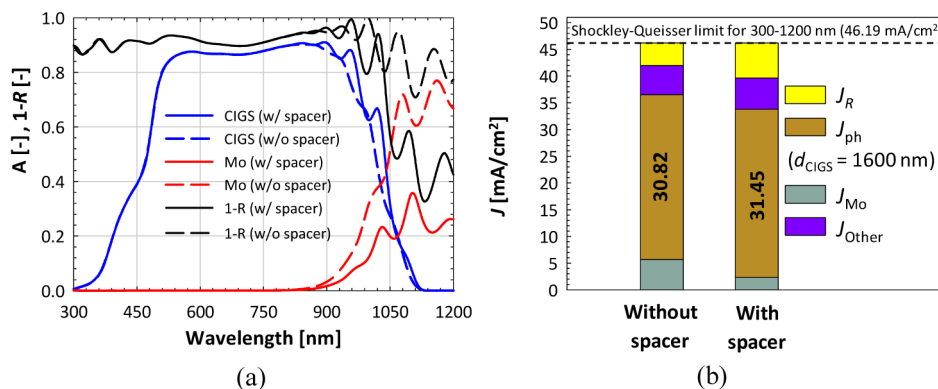
Fig. 9. a) The absorption in 1600-nm thick CIGS (blue) and Mo (red) and 1-R (black) for the reference cell (dashed) and the cell with two-layer spacer (solid), and b) the integrated absorption in different layers of CIGS solar cell for the wavelength range between 300 and 1200 nm.

3.4 Electric field investigation

One of the main advantages of 3D optical simulations over 1D simulations is the possibility to observe electric field distribution in every point of the structure. In order to show that the current enhancement in long wavelength regime is partly resulted from the reduction of

plasmonic resonances [18], the magnitude of electric field ($|\bar{E}|$) is evaluated. Particularly, $|\bar{E}|$ is sampled along the central line of the cell at $\lambda = 1020$ nm, corresponding to the third peak of the solid blue curve in long wavelength range in Fig. 9(a), with and without the spacer for transverse magnetic (TM) light illumination. We looked at this polarization, because surface plasmons can only be excited by TM polarized light [18,24], although in this case, due to the symmetry of the structure, the difference between TE and TM polarizations is not pronounced. Figure 10(a) shows that by inserting the two-layer spacer, $|\bar{E}|$ is increased along the cell, which, according to Eq. (2), leads to the absorption enhancement. The excitation of surface plasmons at Mo / CIGS interface at $\lambda = 1020$ nm can be noticed from the peak of electric field at that interface in Fig. 10(b), which has an almost exponential decay in CIGS (linear decay in logarithmic scale). This observation is in agreement with our discussion in section 3.1. This lossy optical mechanism prevents the reflection of photons from Mo surface back into the absorber, a phenomenon similar to plasmonic losses in Si-based solar cells [36]. It should be noted that according to our studies, this phenomenon could not be observed, if the natural roughness of Mo was not included in the model, which is in agreement with the necessary conditions for the excitation of plasmonic waves. As indicated in Fig. 10(c), instead, the plasmonic resonance is quenched in the modified structure endowed with MgF_2 / Al_2O_3 spacer. In fact, the peak in $|\bar{E}|$ at Mo surface is disappeared, explaining the peak in CIGS absorption in Fig. 9(a) at the corresponding wavelength.

3.5 Point contact optimization

The proposed structure in its current format cannot be a working solar cell, unless the absorber layer is connected to Mo [37] to enable hole collection. Therefore, local point contacts with circular cross sections are added to the structure (see Fig. 11(a)). The radius and spacing between these contacts should be optimized for maximal J_{ph}. However, it should be kept in mind that in a local point contact scheme, the charge carriers move in lateral direction to finally reach the back contact. Therefore, the point contact spacing should be less than twice the minority carrier diffusion length in CIGS layer (between 0.5 and 2 μm [38]) to prevent carrier recombination in the absorber.

As abovementioned, sub-micron CIGS layers are required for reducing material consumption. Accordingly, our point contact scheme was optimized for a cell with 750-nm thick CIGS absorber, re-finding first the best MgF_2 thickness and investigating after different geometric configurations. Due to less absorber thickness, higher energy photons with wavelengths down to 700 nm can reach the back contact. That is why in this part of the contribution results attain the wavelength range between 700 nm and 1150 nm, where the upper bound was chosen based on measured EQE spectrum of the baseline ultra-thin solar cell. We found that the optimal thickness for MgF_2 is 100 nm, which, in combination with a 10-nm thick passivating Al_2O_3, leads to 1.15 mA/cm^2 increase in J_{ph} (or 8.5% improvement for $700 < \lambda < 1150$ nm) compared to the reference cell. The optimized value of MgF_2 thickness is different from the one obtained in [34],because of the different performance indicator (J_{ph} in our case instead of rear reflectance). In fact, increasing the rear reflectance will lead to the improvement of J_{ph}, but not all the reflected light can be absorbed in the absorber and the maximal value of J_{ph} is not necessarily accompanied with maximal rear reflectance. In addition, the optimization in [34] was performed for $800 < \lambda < 1100$ nm, independently from CIGS thickness. In reality, CIGS thickness plays an important role in the wavelength range of photons reaching the back contact, causing the optimization regime vary for different absorber thicknesses.
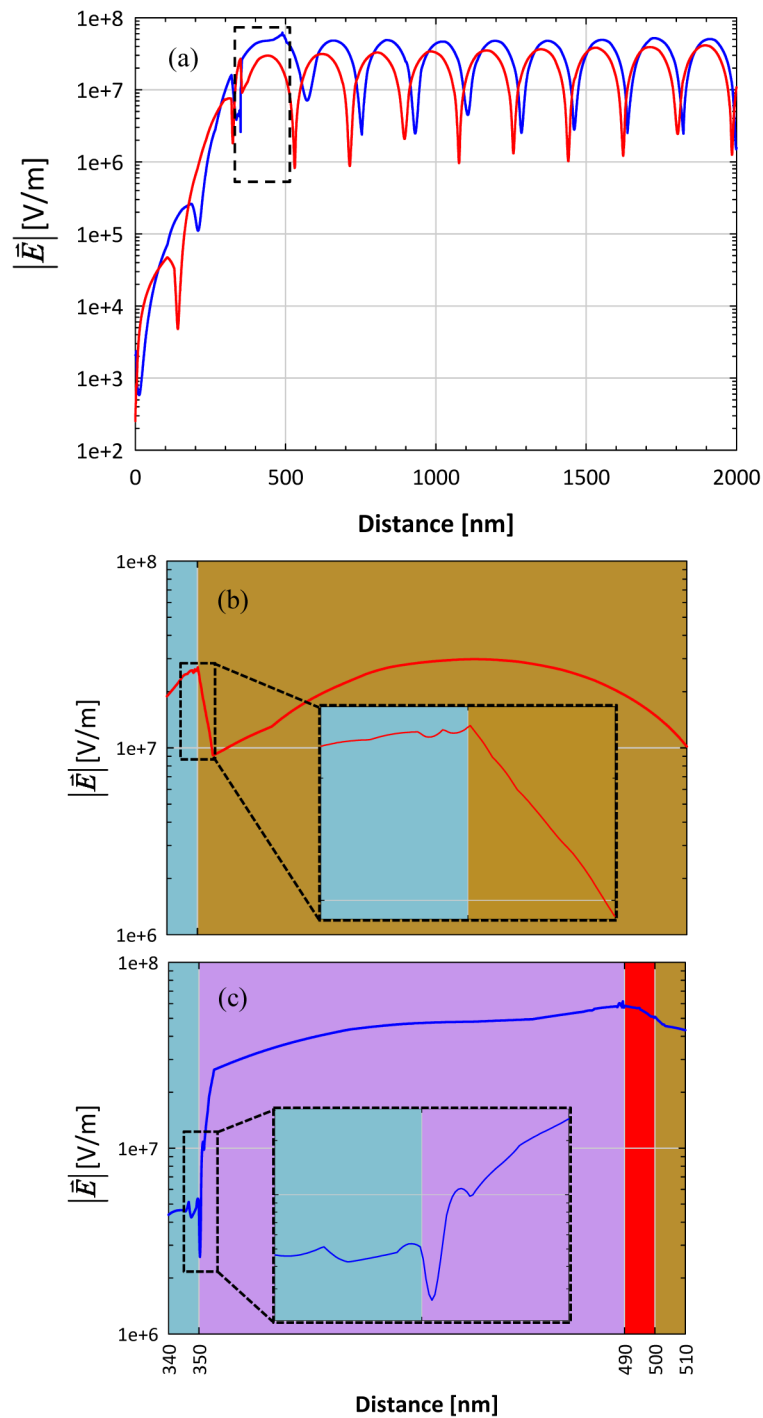
Fig. 10. From top to bottom, magnitude of the electric field $\left|\vec{E}\right|$ along the central line of the solar cell at $\lambda = 1020$ nm as a function of the distance from the back side of the cell for TM illumination: a) comparison between the reference cell (red) and the cell with MgF_2 / Al_2O_3 spacer (blue), b) a closer look at the area shown in the dashed rectangle for reference cell and c) the same but for the cell with MgF_2 / Al_2O_3 spacer. The background colors indicate different layers: Mo (greenish-grey), MgF_2 (pink), Al_2O_3 (red) and CIGS (brown).
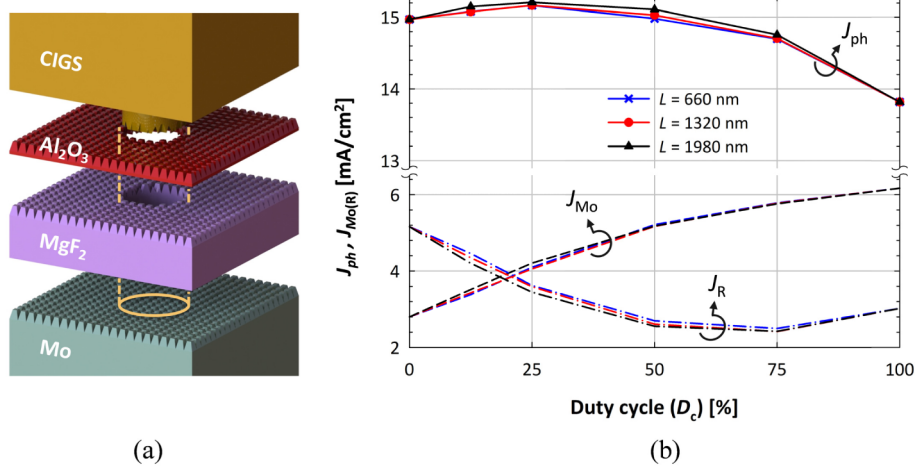
Fig. 11. a) Dual-layer spacer / passivator consisting of MgF$_2$ (100 nm) and Al$_2$O$_3$ (10 nm), including the point contact scheme; b) implied photocurrent density and integrated Mo absorption and reflection loss for $700 < \lambda < 1150$ nm as a function of Duty cycle (D_c) for unit cell lengths of two, four and six times larger than the correlation length of CIGS surface texture.

As for the investigation on different geometric configurations, two structural parameters were varied: the unit cell size (L) and the *Duty Cycle* (D_c). D_c represents the area coverage of point contacts and is defined as $\pi r^2/L^2$, in which r is the radius of the point contact. It should be noted that L is the point contact period too. The smallest value of L is 660 nm, equal to two times larger than the correlation length of as-grown textures on CIGS surface. In Fig. 11(b), J_{ph} and integrated Mo absorption and reflection losses as functions of D_c are shown. 0% and 100% D_c correspond to full passivation and no passivation of the back contact, respectively. It can be observed that there is a trade-off between Mo absorption and total reflection. Current loss due to Mo absorption is minimized when its surface is fully covered with the spacer and increases by increasing the area coverage of point contacts, which is in agreement with the analyses in previous sections.

According to a previous study on diffraction gratings [39], the intensity of diffracted modes depends on duty cycle of the grating and, for $D_c = 50\%$, all diffracted modes are excited altogether, which means that the light is overall diffused in higher angles (with respect to the normal to the interface). This increases the optical path length of light inside the absorber and, hence, results in higher chance of light absorption. By looking at the point contact structure as a diffraction grating, the same interpretation seems to be realistic. Although, for $D_c = 50\%$ more light is diffused outside the escape cone of CIGS layer, this is counterbalanced by more Mo absorption. Accordingly, for less D_c values, less Mo absorption is balanced out by more light escaping the solar cell (more total reflection). It can be concluded from Fig. 11(b) that these two parameters reach an optimal point close to $D_c = 25\%$, leading to maximal light absorption in CIGS layer.

The presence of a similar trend for different point contact periodicities shows the scalability of the structure. It means that it is possible to fabricate this structure using techniques that are cheaper than e.g. e-beam lithography. For the case of $L = 1980$ nm, the current density improvement at optimal D_c is 1.39 mA/cm^2 (or 10%) for the wavelengths between 700 and 1150 nm. The simulations for the whole spectral range of interest indicate that J_{ph} is improved by 1.45 mA/cm^2, from 28.04 to 29.49 mA/cm^2, which can be translated to a 5.27% optical improvement.

4. Conclusions

An optical model of a CIGS solar cell using 3-D Maxwell equation solver based on the finite element method was presented. The software was calibrated with the measured EQE and R spectra and a qualitative agreement was obtained. The natural textures of different layers were modeled by truncated pyramids.

The possibility of the excitation of SPPs at Mo / CIGS interface was investigated by studying the dispersion curve. Results show that for a wide wavelength range in the visible part of the spectrum, leaky surface waves can be excited at a flat Mo / CIGS interface. In the long wavelength range, on the other hand, the presence of natural roughness on Mo facilitates the excitation of surface-bound plasmons, dramatically reducing the EQE.

Borrowing the concept of dielectric spacer from Si PV technology, the insertion of a synthetic low refractive index dielectric layer between Mo and CIGS was optically studied. It was shown that (i) such a spacer will quench the optical losses caused by high absorption in Mo and plasmonic losses in long wavelength regime and (ii) an optimal thickness for the dielectric spacer exists. The capability of Al_2O_3, which is the state-of-the-art material in CIGS-based PERC-like structures, in enhancing J_{ph} was compared to that of MgF_2. The results indicate that the latter - with the optimal thickness of 140 nm - performs better than Al_2O_3.

Then, a two-layer spacer / passivator consisting of MgF_2 and Al_2O_3 was designed and the thickness of MgF_2 was optimized for maximum J_{ph}. An absolute increase in J_{ph} by 0.63 mA/cm^2 for the whole visible spectrum can be expected with the proposed structure, notwithstanding increased reflectance losses. These are, in fact, closely related to augmented absorptance in CIGS when Mo optical losses are quenched. A study on the magnitude of the electric field proves that the *plasmonic losses* are quenched by the two-layer spacer, giving rise to better light absorption in the CIGS layer.

Finally, point contacts were inserted into the cell structure endowed with a 750-nm thick CIGS absorber and their area coverage was optimized for maximal implied photocurrent density. The results indicate that the trade-off between current loss in Mo and total reflection is balanced out for $D_c = 25\%$, leading to improvement of J_{ph} by 10% compared to the reference cell for the wavelengths between 700 and 1150 nm.

Acknowledgments